CHAPTER 4

HIGH-TEMPERATURE SOLID PARTICLE EROSION OF TYPE 446 STAINLESS STEEL

4.1 INTRODUCTION

In the present work, we aim to investigate the behavior and performance against the erosion of Type 446 stainless steel under high operating temperatures and variable impact angles. In Suur's studies of the dependence between the wear rate and temperature, it was illustrated that the wear rate barely shows any change up to 450°C. With the increase in temperature up to 450°C, a hard protective layer of Fe_2O_3 prevents erosion whereas beyond 570°C a weak film of FeO which combines with the parent metal causes a steep rise in the erosion rate [156]. This response of materials towards high-temperature erosion and the application of Type 446 stainless steel when used in the tubes working with temperature in the range of 200°C to 800°C restrict the investigators to observe the behavior in the specified temperature zone. The effect of microstructure on the erosion of Type 446 stainless steel is investigated under ambient conditions and elevated temperature conditions using erosion test rig similar to that shown in ASTM G76-95 standard. Various operating conditions with a discharge rate of 4.2 ± 0.5 gm/min and particle velocity of 100 m/s were employed at impact angles of 30˚, 60˚, and 90˚. The micro-hardness test carried out for the sectioned eroded sample indicates the hardening effect along with the cross-sectional depth, which inversely affects the erosion rate. It was found in agreement with previous theories that Type 446SS showed higher erosion resistance at normal impact than oblique impacts in case of ambient conditions, whereas, under elevated temperature conditions increasing trend in erosion was seen. Surface and

sub-surface examinations were carried out using SEM, 3D-profilometer, and surface roughness analyzer. Ploughing, metal cutting, indentation and crater formation are the mechanisms primarily responsible for erosion, indicating severe erosion at 30˚ impact angle. It was also observed that under high temperature working conditions dissolution of carbides precipitates occurs which affects the mechanical properties of the material, as already discussed in Chapter 3.2.

4.2 RESULTS AND DISCUSSION

4.2.1 Erosion Mechanism

To wear out the material from the surface, the impact energy [Eq. (4.1)] should be greater than the proof force per unit area [Eq. (4.2)]. The impact of particles displaces the material from impact sites into the raised crater, rims and lips causing detachment from the surface by the plastic rupture in the form of wear debris. This is the cause of an increase in erosion rate initially. Subsequently, under the effect of repeated impacts, surface hardening takes place, and thereby the erosion rate is sustained at a constant value.

$$E_T = E_k + E_p = \tfrac{1}{2} mv^2 + mgh \quad (4.1)$$

$$F = \pi r^2 \sigma \quad (4.2)$$

The impingement of particles on the surface may undergo particle fragmentation, surface shielding due to rebounding particles, and particle embedding effects among others. The net erosion rate is an outcome of the relative contribution of the different mechanisms under several mechanical properties [157,158]. Properties used for correlations such as tensile toughness, work hardening exponent, strength coefficient and hardness are most likely to vary with temperature change. The effects of increasing temperature on erosion have been studied in more detail in the last few years. Finnie et

al. [159] reported increased erosion for increased temperature contrary to which Smeltzer et al. [160] reported the decrease in erosion with increasing temperature for other alloys.

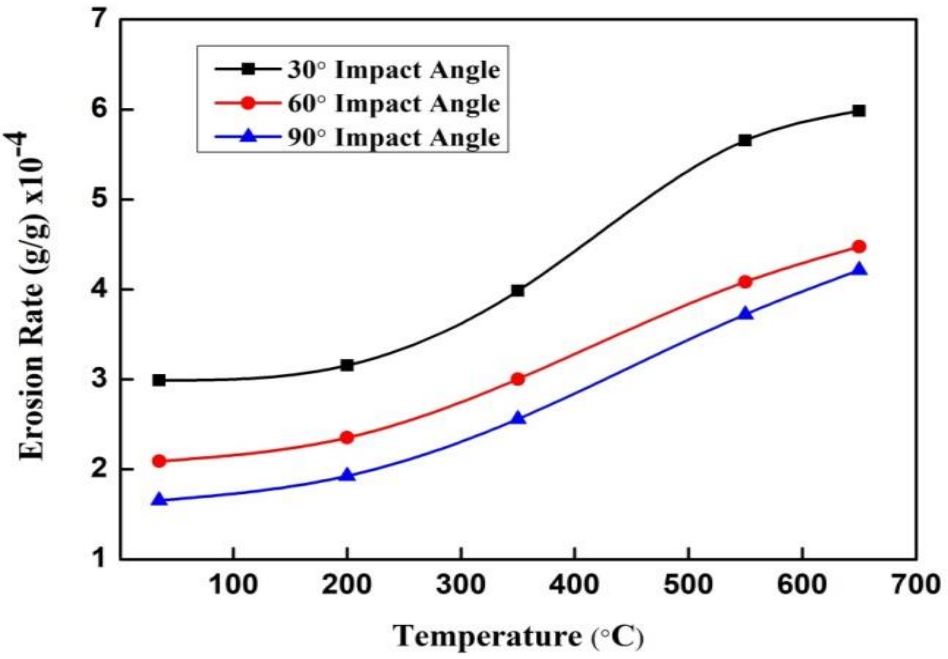

Fig. 4.1: Dependence of ER on the temperature at an impingement angle of 30º, 60º and 90º.

The temperature dependence of erosion rate on Type 446SS at the impact angle of 30°, 60°, and 90° is shown in Fig. 4.1. The curve shape under all the impact angles is closely identical, with erosion rate being maximum at 30° and minimum at a normal impact. This is typically identified as the behavior of the ductile material. Also, the effect of temperature is prevalent in the erosion of the material. It is well observed that with the increase in temperature there is certainly an increase in the erosion rate, however, this can not be thought of as linear dependency. It is well observed that with the increase in temperature there is certainly an increase in the erosion rate, however, this can not be thought of as linear dependency. It is noted that the increase in ER is less significant up

to 350ºC, whereas in the range of 350ºC to 550ºC a steep slope is observed which is indicative of higher ER.

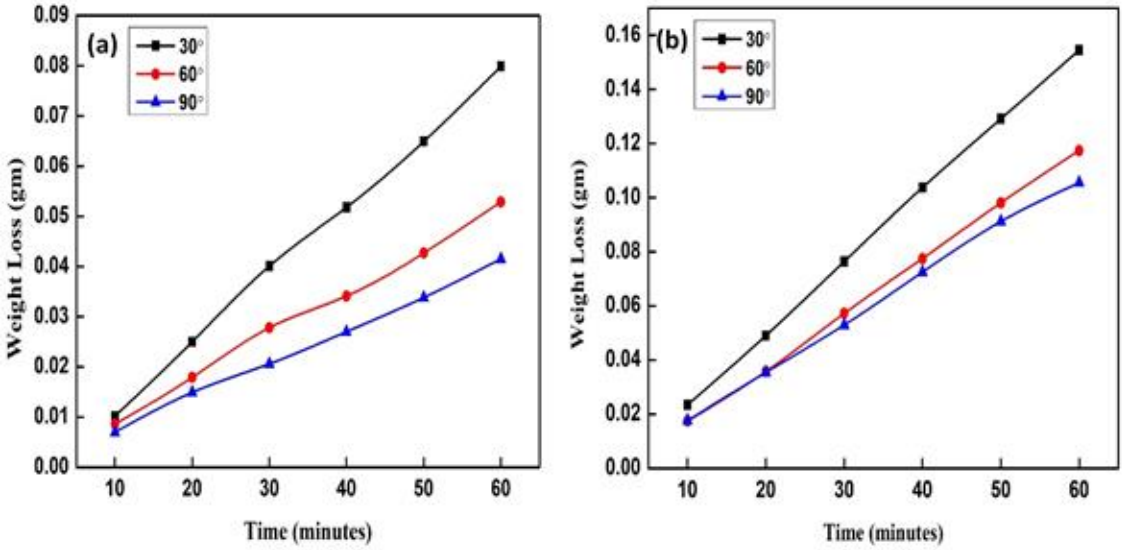

Fig. 4.2: Weight loss vs. time for Type 446SS at variable impact under **(a)** RT and **(b)** 650°C.

With a further increase in temperature, it is seen that ER is almost steady between 550ºC to 650ºC. This can be due to abrasive bonding to the eroded surface which offers protection from further impacts.

The erosion sample subjected to testing undergoes the loss of weight under the impingement of different impact angles at 100 m/s. The cumulative weight loss measured after every 10 minutes is plotted in (Fig. 4.2) to represent the cumulative weight loss with the increase in test duration. The curve showed maximum erosion of the specimen under oblique impact than normal impacts. Depending upon the angle of incidence, different erosion mechanisms may act alone or coexist in interaction resulting in measured weight loss. All such mechanisms are identified with the help of SEM. Fig. 4.3 shows the macrograph and 3D interactive plot of the scar on the tested material under variable impact angles. The elliptical shape is seen at the oblique impact of 30° angle whereas the

normal impact of 90° showed an approximate circular scar. The orientation of the specimen at different impact angles and divergence of the particle stream leads to the formation of different impact geometry. The plumes of the impinging particles are concentrated in the central part of the stream. At all impingements, the halo effect which is characterized by secondary erosion damage is seen.

The depth of scar formed at each impact angle under each tested condition is measured using (Mitutoyo) surface roughness tester. Along with, depth profile and contour of tested samples at 30°, 60°, and 90° is shown in Fig 4.4.

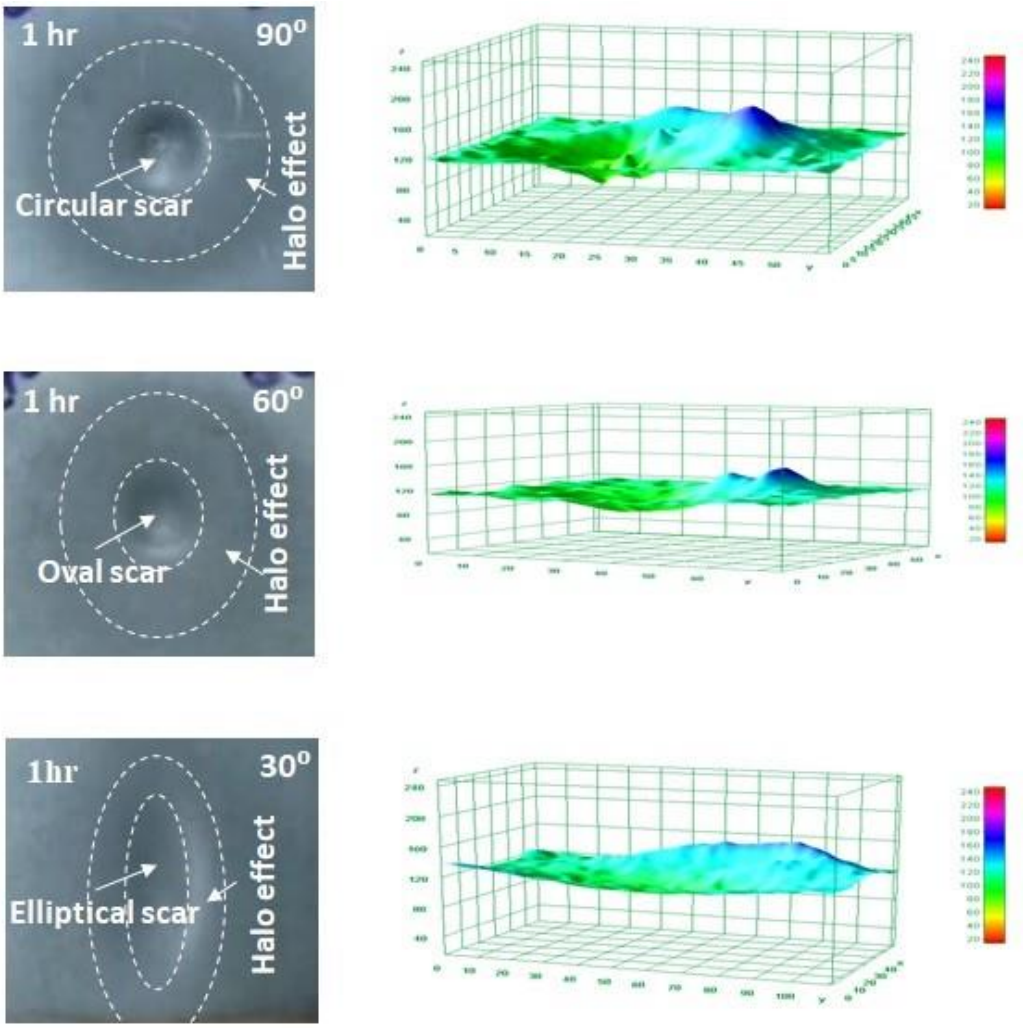

Fig. 4.3: Wear scar and 3D interactive plot of the tested material

The erosion rate at oblique impact is maximum, but the average surface roughness (R_a) is maximum in case of the normal impact shown in Table 4.1. This is likely to happen since the normal impact created many pits on the surface, thereby squeezing the material forming more ridges. Thus the consolidated effect of pits and ridges turnout in the form of higher surface roughness.

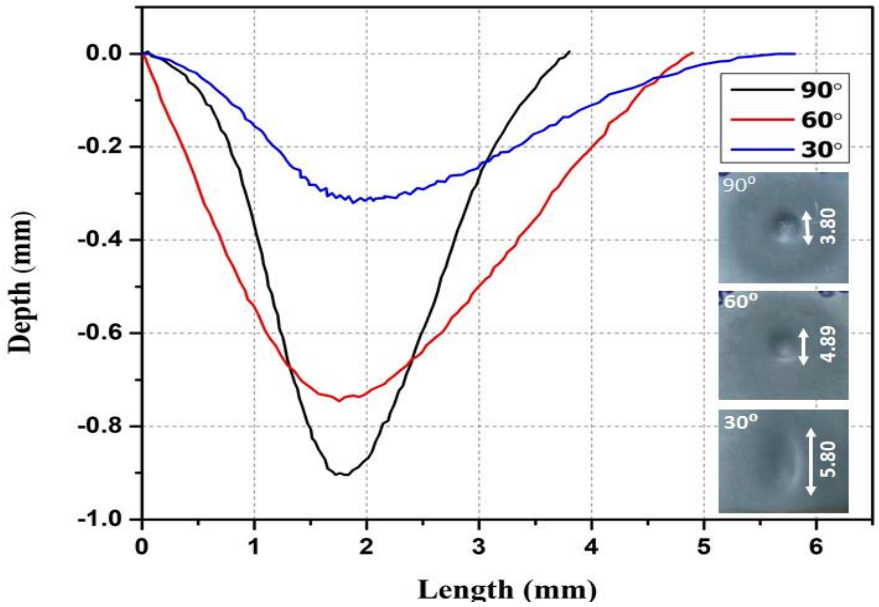

Fig. 4.4: Erosion scar profile comparison for 30º, 60º and 90º angle of incidence after 1hr test at 650ºC.

Table 4.1: Properties of the eroded surface at 650ºC

Angle (°)	30°	60°	90°
Erosion Rate (g/g)x10^{-4}	5.98±0.41	4.47±0.33	4.22±0.46
Depth of cut (μm)	322±15	746±11	907±16
R_a (μm)	6.64±2	14.23±3	24.09±5

A further investigation is carried out on the sample by measuring the hardness along the cross-section beneath the scars to identify the effect of work hardening beneath the surface which suffers the repeated impact.

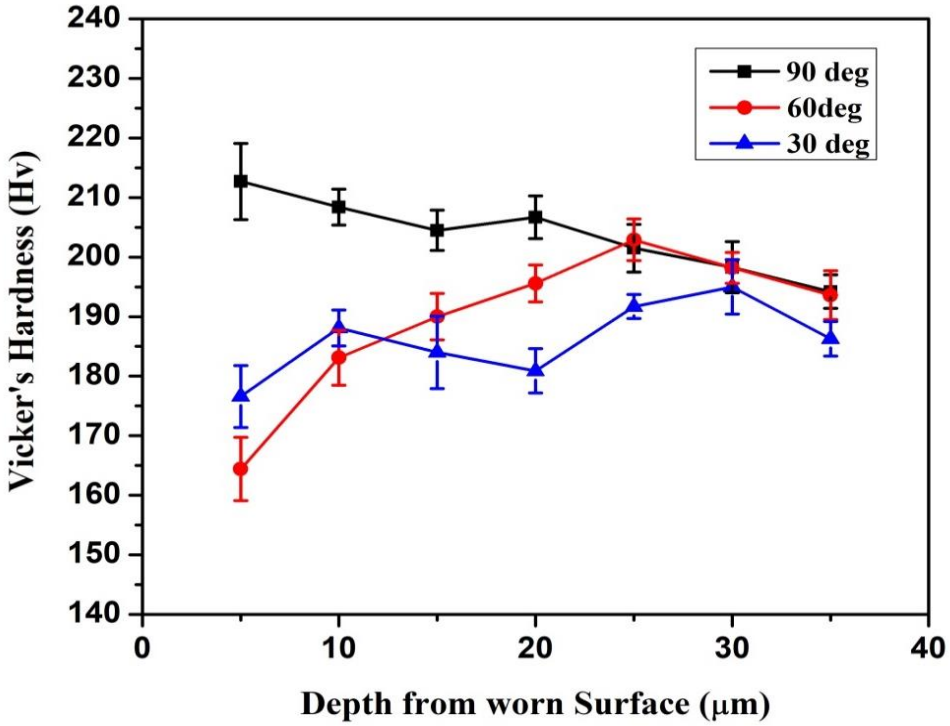

Fig 4.5: Hardness along the cross-section to impact surface

There is no definite trend seen in the hardness of the surface along the cross-section as clear from Fig. 4.5. However, under the normal impact, hardness increase is more significant than the oblique impact. Hardness in each case approaches the hardness of as-received conditions, i.e., 193 HV with the advancement in depth. This signifies that the impact of particle created work hardening effect to depth off ~30 μm below the surface. The topography of the worn-out sample is shown in Fig. 4.6.

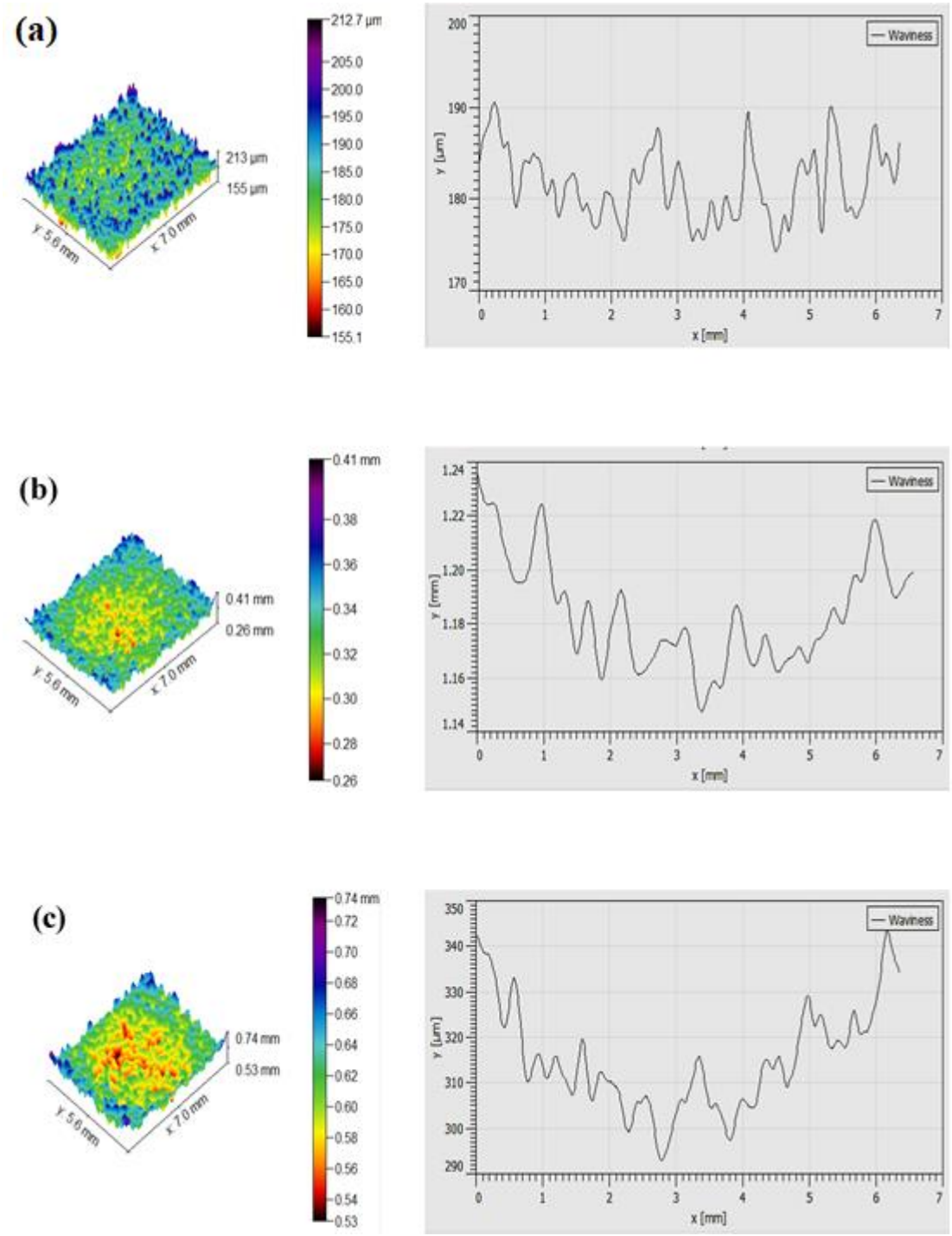

Fig 4.6: Worn surface topography of tested sample at RT: **(a)**30º **(b)** 60º, and **(c)** 90º.

SEM analysis of the eroded surface, as shown in (Fig.4.7) is an attempt in the identification of the mechanism responsible for the loss of material under different impact conditions. "Low angle metal cutting" mechanism is the most prominent mechanism which operates in conjunction with micro-cutting/ploughing and plastic deformation

when subjected to low impact angles and high velocity [161]. Fig. 4.7(a) shows the lips and the sharp groove formed due to cutting mechanism when impacted at 30º at room temperature conditions whereas at 650ºC the grooves are shallow but the lips formation is more prevalent (Fig 4.7(b)), and therefore, the loss of material is higher. The sharp angular particles when striking the surface with such a high velocity of 100 m/s, the kinetic energy associated with them is relatively high to overcome the critical energy required for cutting. As a result, the material is collected as a ridge and lips on the trailing edge of the narrow groove. With the subsequent impact, work hardening of these ridges takes place, and thereby fractures and removal of material in the form of wear debris are seen in the later stage. This mechanism is also applicable to high-temperature impact conditions. However, due to a change in material properties at elevated temperatures, there is a higher loss of the material. The high-temperature tensile test indicates that with the increase in temperature there is the initial drop in ductility up to 350°C, however, with further increase in temperature up to 650°C the ductility is increasing. This initial drop in ductility is attributed to dynamic strain aging behaviour.

Fig. 4.8(a-b) shows the characteristics of the surface under a higher impact angle. It is observed that both shallow and deep craters are formed on the surface along with some indentation marks. EDX results indicated that the craters are filled with wear debris of the material and erodent as well. This effect is also seen at the 650ºC temperature as shown in (Fig. 4.8(b)) where the craters are more elongated, and the scratch marks are dense. Fig. 4.9(a-b) shows the observation under normal impact and is explained on the grounds of kinetic energy associated with the impact. The component of kinetic energy associated with high velocity is large in the normal direction. This helps the sharp angular particles of Al_2O_3 to impact on the surface and squeezes the material on sides of the dimples. In the influence of repeated impact, these particles develop the crack and are

eventually removed in the form of debris. These Al_2O_3 particles act as a protective shield from the incoming impact and also deflect them in a random direction. This deflection leads to removal in the form of small wear debris which is identified as "Secondary metal cutting."

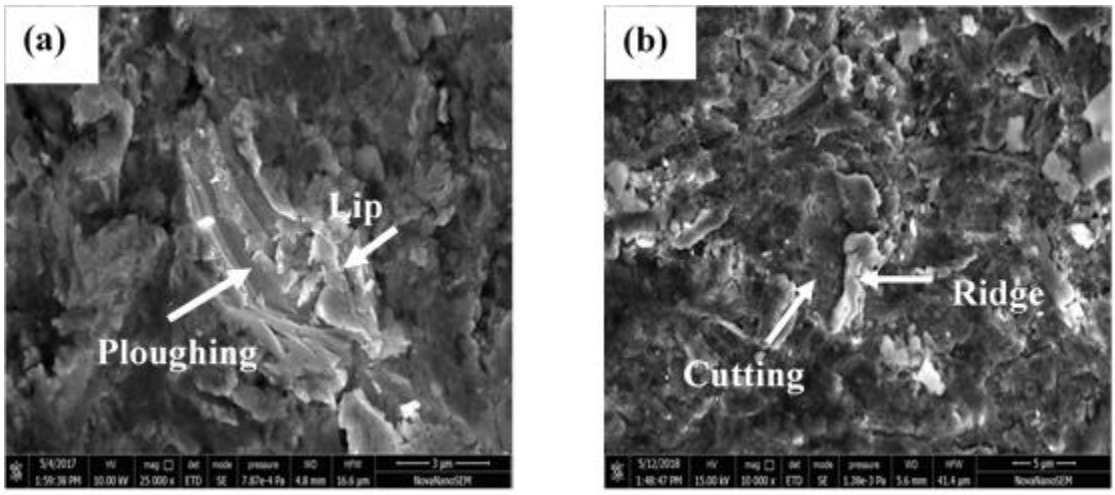

Fig. 4.7: SEM micrograph of eroded scar at 30º under **(a)** RT **(b)** 650°C.

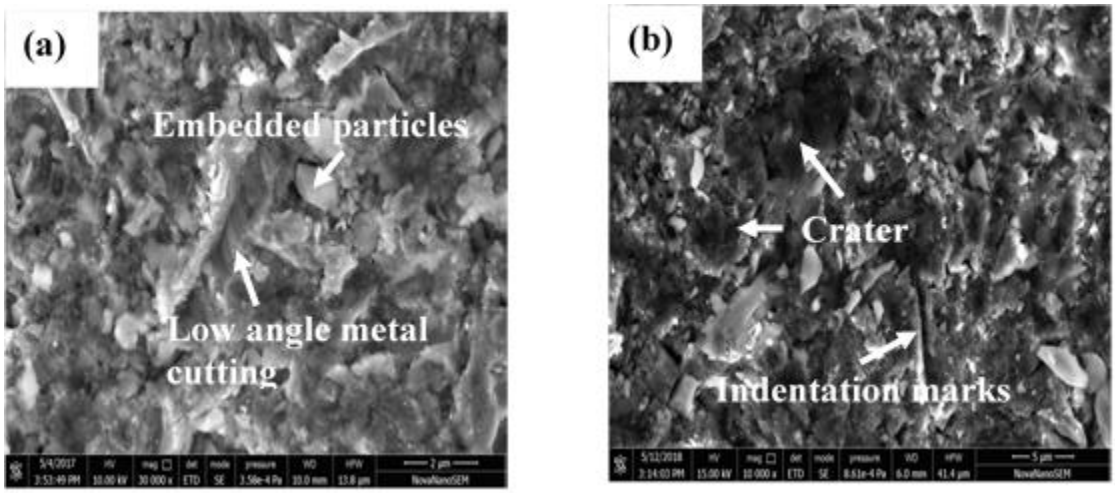

Fig. 4.8: SEM micrograph of eroded scar at 60º under **(a)** RT **(b)** 650°C.

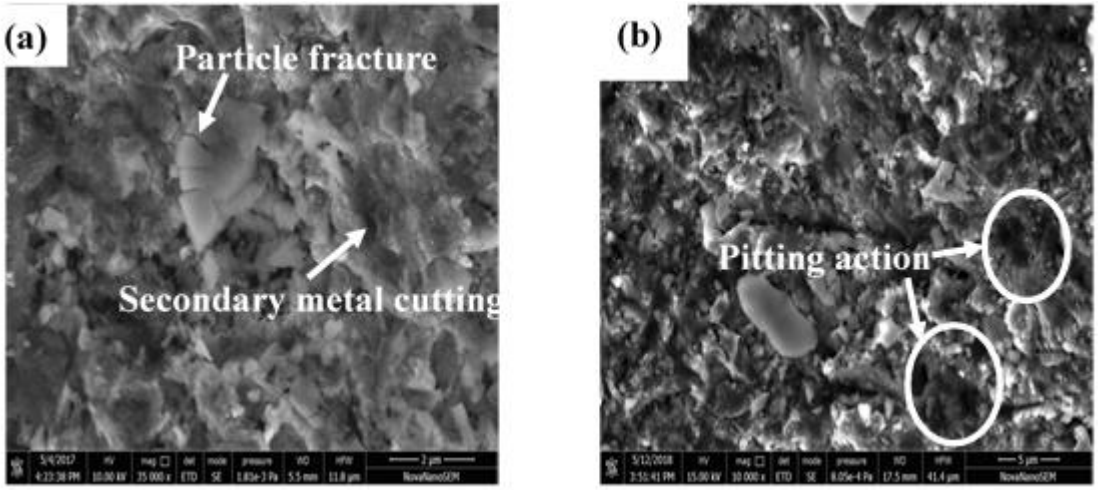

Fig 4.9: SEM micrograph of eroded scar at 90º under **(a)** RT **(b)** 650℃.

Cross-Sectional observation of Type 446SS undergone oblique impact is shown in Fig. 4.10(a-b). SEM micrograph reveals that the crests of the ripples are cut by impacting abrasives. The formation of ripples on the wearing surface is perpendicular to the direction of the velocity vector under the effect of abrasive particle impact causing plastic deformation directed along the velocity vector. The geometry of the ripples is dependent on velocity and fraction of the abrasives. Although, this ripple pattern is generally seen in oblique impacts, yet they are seen with lost coherency in normal impact conditions too. The wavelength of the protrusion formed on the crests of the ripple was approximately 180 μm. It is also seen that elevated temperature tests increased the wavelength of the ripples thereby indicating the direct dependence on temperature.

4.2.2 Characteristics of oxidation and properties of oxide scale

The iron alloy containing Cr > 20 wt% form sesquioxide scale traditionally called "protective". X-ray diffraction demonstrated that very thin featureless scale and somewhat smaller grains of α-M_2O_3 type oxide forms on high chromium alloys [162].

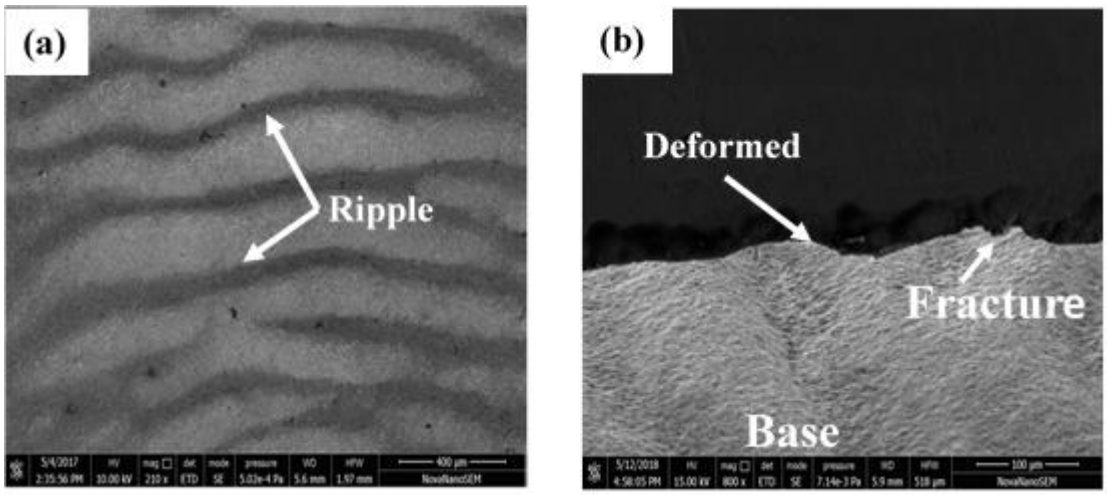

Fig 4.10: (a) SEM micrograph of eroded scar at 30º and **(b)** cross-section profile of the near surface of 446SS at 650℃ and 30º impingement angle.

Steels with Cr > 10 wt% forms segmented and thin Cr_2O_3 scales formed during erosion leading to low erosion rate [163]. As shown in (Fig. 4.11(a)) ferritic alloy oxidized to give outer Cr_2O_3 oxide with smaller grain size. SEM examination of the oxide surface showed many chromium-rich nodules formed within the dimple when exposed to air at 650ºC for 10 min. These oxide crystallites initiate and grow preferentially in the defect locations. In Fig. 4.11(b), the oxide is seen to grow in and away from the metal surface and the nodules are characterized by the model like the growth of blades and whiskers. This oxide scale formed does not contribute to significant weight gain and is neither uniform not continuous due to the slow oxidation rate at this temperature. Due to its sparse nature, this oxide scale does not play any significant role in the elevated temperature process. Thus variation in erosion rate with temperature is due to change in temperature-dependent properties of the material.

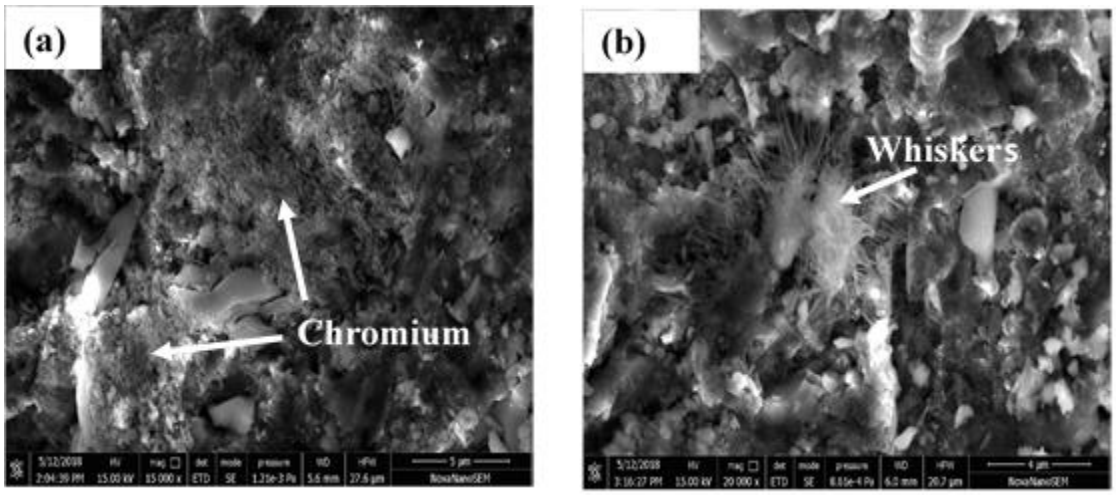

Fig. 4.11: (a) and **(b)** SEM micrograph of oxide nodules formed on 446SS during erosion test.

4.3 CONCLUSIONS

Following are the conclusions drawn from the present investigation:

1. The variation of erosion rate with temperature is similar under all temperatures. It remains virtually unchanged up to 350℃ and follows a sharp increase up to 550ºC before stabilizing with moderate erosion rate at 650℃.
2. Morphology of erosion changes with test temperature. The grooves indentation, craters, and plough marks are larger when impacted at a higher temperature in comparison to room temperature.
3. The oblique impact showed consistent ripples formed due to the plastic flow of material. These ripples changed to deranged scars for higher impact angles.
4. The role of oxidation is insignificant between RT and 650ºC. These oxides are non-uniform. The variation of erosion with temperature in this temperature range may be explained in terms of the changes in tensile strength with temperature and precipitation of carbides in the grain boundary region.

